JGR Atmospheres

RESEARCH ARTICLE
10.1029/2021JD035812

Recent Changes of Pacific Decadal Variability Shaped by Greenhouse Forcing and Internal Variability

Weiyi Sun[1], Bin Wang[2,3], Jian Liu[1,4,5], and Yifei Dai[6,7]

[1]Key Laboratory for Virtual Geographic Environment, Ministry of Education, State Key Laboratory Cultivation Base of Geographical Environment Evolution of Jiangsu Province, Jiangsu Center for Collaborative Innovation in Geographical Information Resource Development and Application, School of Geography Science, Nanjing Normal University, Nanjing, China, [2]Department of Atmospheric Sciences and Atmosphere-Ocean Research Center, University of Hawaii at Manoa, Honolulu, HI, USA, [3]Key Laboratory of Meteorological Disaster of Ministry of Education and Earth System Modeling Center, Nanjing University of Information Science and Technology, Nanjing, China, [4]Jiangsu Provincial Key Laboratory for Numerical Simulation of Large Scale Complex Systems, School of Mathematical Science, Nanjing Normal University, Nanjing, China, [5]Open Studio for the Simulation of Ocean-Climate-Isotope, Qingdao National Laboratory for Marine Science and Technology, Qingdao, China, [6]Key Laboratory of Transportation Meteorology, CMA, Nanjing, China, [7]Nanjing Joint Institute for Atmospheric Sciences, Nanjing, China

Key Points:

- Observed Pacific Decadal Variability (PDV) has weakened over the South Pacific and Kuroshio-Oyashio Extension while amplified over the northeast Pacific horseshoe-like region since 1999
- Greenhouse gases forcing has a potential impact on weakening the PDV, which is also suggested by future warming scenario
- The increased PDV over the eastern boundary North Pacific and central Pacific may be associated with internal variability

Supporting Information:

Supporting Information may be found in the online version of this article.

Correspondence to:

J. Liu,
jliu@njnu.edu.cn

Citation:

Sun, W., Wang, B., Liu, J., & Dai, Y. (2022). Recent changes of Pacific decadal variability shaped by greenhouse forcing and internal variability. *Journal of Geophysical Research: Atmospheres*, *127*, e2021JD035812. https://doi.org/10.1029/2021JD035812

Received 5 SEP 2021
Accepted 25 MAR 2022

Author Contributions:

Conceptualization: Weiyi Sun, Bin Wang, Jian Liu
Data curation: Weiyi Sun, Yifei Dai
Formal analysis: Weiyi Sun
Methodology: Weiyi Sun
Software: Yifei Dai
Supervision: Jian Liu
Validation: Yifei Dai
Writing – original draft: Weiyi Sun
Writing – review & editing: Weiyi Sun, Bin Wang, Jian Liu

Abstract Pacific Decadal Variability (PDV) has enormous influences on North American and Eurasian climate and Pacific ecosystems. Its change under anthropogenic warming is of prodigious societal concern and scientific dispute. We show evidence that the observed PDV has amplified in the northeast Pacific horseshoe-like region while weakened over the South Pacific and Kuroshio-Oyashio Extension (KOE) region since the beginning of the 21st century. Congruently, under the influence of PDV, precipitation anomalies have significantly amplified globally and reversed the sign over Africa and East Asia. Analysis of the Coupled Model Intercomparison Project Phase 6 (CMIP6) historical simulations and future projections suggests that greenhouse forcing weakens the PDV in the South and northwestern Pacific and shortens its periodicity. However, the observed PDV's enhancement over the North Pacific eastern boundary is likely due to internal variability. Our findings on the PDV's response to anthropogenic forcing and internal variability shed light on the PDV's future change and decadal prediction.

Plain Language Summary Pacific Decadal Variability (PDV) is one of the primary modes of internal variability. There is an unprecedented change of the PDV after 1999, which reveals a sudden change in the spatial pattern, intensity, and climate impacts of the PDV. The amplitude of PDV has decreased over the South Pacific and Kuroshio-Oyashio region but strengthened along the west coast of North America and equatorial central Pacific. This current PDV's cycle has amplified the land precipitation anomalies worldwide and reversed the precipitation anomalies over Africa, East Asia, and sub-Arctic regions. We used the Coupled Model Intercomparison Project Phase 6 multi-model results to illuminate that the recent unprecedented change of the PDV may be influenced by the combination of greenhouse warming and internal variability. Our findings reflect an advance in understanding the long-term changes of the PDV and its remarkable impact on global land precipitation.

1. Introduction

Pacific Decadal Variability (PDV) has profound impacts on the Pacific ecosystems and the climate variability in Eurasia and North America (Dai, 2013; Liguori & Di Lorenzo, 2018; Liu, 2012; Liu & Di Lorenzo, 2018; Whitney, 2014). The term PDV used here includes the Pacific Decadal Oscillation (PDO) (Mantua et al., 1997), Interdecadal Pacific Oscillation (IPO) (Power et al., 1999), and South Pacific Decadal Oscillation (SPDO) (Mo, 2000). Although IPO is defined in different domains, its temporal variation is highly correlated with PDO/SPDO (Liu & Di Lorenzo, 2018).

Previous studies analyzed the PDV before 2013 and contrasted PDV's climate impacts between its positive and negative phases (Lyon et al., 2014; Qin et al., 2018), and linked PDV with various climatic dynamic processes (Newman et al., 2016). The tropical forcing can be considered one of the drivers (Deser et al., 2004). The El Niño-Southern Oscillation (ENSO) was found to affect the Aleutian Low variability through the atmospheric bridge (Alexander, 1992; Alexander et al., 2002) or seasonal footprinting (Deser et al., 2012; Vimont et al., 2001),

contributing to the PDV. Modeling results suggested that an enhanced ENSO variability may affect the intensified variance of tropical PDV (TPDV) and the relationship between ENSO and PDO could become stronger in future (Choi et al., 2013; Kwon et al., 2013). Meanwhile, using the Geophysical Fluid Dynamics Laboratory (GFDL) model, some studies found that the bi- and multi-decadal PDO mode can be affected by mid-latitude air-sea interactions via the westward propagating oceanic Rossby waves (Zhang & Delworth, 2016; Zhong et al., 2008). Over the past two decades, despite the interruption of global warming during 1999–2013, the global ocean heat content has experienced accelerated warming, with the most massive warming in the tropical/subtropical Pacific Ocean, the southern oceans, and the global subtropical western boundary currents (Cheng et al., 2017; Liu et al., 2016; Lyman et al., 2012; Wu et al., 2012). Therefore, it remains unknown whether the extensive oceanic warming influences the PDV's positive and negative phases since 1999.

An unprecedented warm sea surface temperature (SST) occurred over the northeastern Pacific after 2014, causing the most extensive marine heatwave ever recorded (Amaya et al., 2020; Di Lorenzo & Mantua, 2016). Some studies found that the atmospheric variability might have initiated the northeastern Pacific warming during the winter of 2013/2014, and the atmospheric forcing might have a tropical origin (Hartmann, 2015; Hu et al., 2017; Seager et al., 2015; Wang et al., 2015). The persistence of the northeastern Pacific warming was related to a warm phase of North Pacific Gyre Oscillation (NPGO) and PDO (Di Lorenzo & Mantua, 2016). The NPGO can be influenced by stochastic variability and central Pacific warming (Di Lorenzo et al., 2010). Note that these investigations focused on the interannual time scale. However, the persistence of the northeast Pacific heatwaves after 2014 might suggest a sign of decadal variability change.

The Coupled Model Intercomparison Project 5 (CMIP5) models show that the near-term predictions of the PDV were essentially model-dependent. The projections had yielded inconsistent results (Van Oldenborgh et al., 2012). For example, some studies with the Community Earth System Model Large Ensemble (CESM-LE) proposed that the variances of the PDO and tropical PDV would increase in a warmer climate (Di Lorenzo & Mantua, 2016; Liguori & Di Lorenzo, 2018). On the other hand, other CMIP5 model studies suggested a reduced PDO's magnitude and periodicity under greenhouse warming (Geng et al., 2019; Li et al., 2020; Zhang & Delworth, 2016). To our knowledge, no study draws attention to the change of the decadal SST variability over the South Pacific in the future warming. However, it is an essential part of the PDV.

Therefore, two questions will be discussed in this paper: (a) Has the PDV's property and impact changed since 1999? (b) What are the potential impacts of external forcings and internal variability on the PDV change, if any?

2. Methods

2.1. Observational Data

The ensemble mean of two sets of SST data is used in this study. One is the Extended Reconstructed Sea Surface Temperature, version 5 (ERSST v5) global SST monthly data on a $2° \times 2°$ horizontal grid (Huang et al., 2017). Another is the Hadley Center Sea Ice and SST data set version 1.1 (HadISST 1.1) with a $1° \times 1°$ resolution (Rayner et al., 2003). We use the Global Precipitation Climatology Center (GPCC) data set overland on a $1° \times 1°$ grid (Schneider et al., 2014). The atmospheric circulation fields are derived from the European Center for Medium-Range Weather Forecasts (ECMWF) reanalysis data set by merging the ERA 40-year reanalysis (ERA-40) during the period 1958–2001 (Uppala et al., 2005) and the ERA-5 reanalysis during the period 1979–2019 (Hersbach et al., 2018). To ensure data consistency, we combine the ERA-40 and the ERA-5 data by calibrating the ERA-40 based on the monthly climatology of the ERA-5 during the overlap period (1979–2001). All variables are detrended during this period.

2.2. Model Data

To investigate the potential impacts of external forcings and internal variability on the PDV change, we use the 33 CMIP6 coupled global climate models' historical runs, pre-industrial (PI) runs, and the 13 models' sensitivity experiments forced by natural (NAT) and greenhouse gases (GHGs) forcings, respectively (Eyring et al., 2016). The temporal coverage is from 1900 to 2005 in the historical experiments, while the results during the last 200 years are used in the pre-industrial experiments.

To further explore the influence of greenhouse warming on the PDV, we examine 33 CMIP6 models' results under the Shared Socioeconomic Pathway 5–8.5 (SSP5-8.5) scenario. The temporal coverage is from 2020 to 2100 in the SSP5-8.5 runs. The observational and models' data are aggregated to a grid resolution of 2.5° latitude by 2.5° longitude using bilinear interpolation. The SST linear trend is removed and processed by a 7-year low-pass filter before analysis.

2.3. First Baroclinic Oceanic Rossby Wave Speed

The SST decadal variability is associated with the adjustment of ocean gyre circulation through the westward propagating Rossby waves (Kwon & Deser, 2007; Newman et al., 2016; Schneider et al., 2002). In a warmer climate, the phase speed of the first-baroclinic oceanic Rossby wave is projected to increase over the North Pacific, which alters the time scale and amplitude of the PDO (Geng et al., 2019; Li et al., 2020; Zhang & Delworth, 2016). In this study, we examine the first baroclinic Rossby wave speed over the entire Pacific (outside of the equatorial band) under the historical and greenhouse warming scenarios from CMIP6 models. Following the method proposed by Chelton et al. (1998), the n-mode Rossby radius of deformation can be defined by

$$\lambda_n = \frac{1}{n\pi|f|}\int_{-H}^{0} N(z)\,dz, \quad n \geq 1, \tag{1}$$

where $f = 2\Omega sin\vartheta$ represents the Coriolis parameter for latitude ϑ and earth rotation rate Ω, H is the depth of the local water, and $N(z)$ denotes the buoyancy frequency, which can be further expressed as

$$N^2(z) = -\frac{g}{\rho}\frac{\partial\rho}{\partial z} - \frac{g^2}{c_s^2}, \tag{2}$$

where ρ is the water density, c_s is the sound speed. The first baroclinic oceanic Rossby wave speed ($C_1 = -\beta\lambda_1^2$) can be written as

$$C_1 = -\beta\left[\frac{1}{\pi|f|}\int_{-H}^{0} N(z)dz\right]^2 \tag{3}$$

where β denotes the meridional gradient of the Coriolis parameter f.

3. Remarkable Changes in PDV Since 1999

Previous studies defined the PDV as the leading empirical orthogonal function (EOF) mode of the low-pass filtered SST anomalies (SSTA) over the Pacific basin (45°S–65°N) (Liu & Di Lorenzo, 2018). Some studies suggest the South Pacific decadal variability could extend to about 60°S (Hus & Chen, 2011; Zhang et al., 2018). To describe the decadal variability over the entire Pacific, we depict the PDV using the first EOF mode of SSTA over the whole Pacific basin (70°S–70°N) (Figure 2a) and define the PDV index using the time series of the first principal component. We use the 7-year low-pass filtered data to obtain the PDV index (Figure 1a). The PDV index is similar to the PDO (SPDO) index derived by using the data north of the 20°N (south of the 10°S), with a correlation coefficient of 0.90 ($p < 0.01$) between them during 1901–2019.

After 1958, the PDV index shows two cold (negative) phases (1961–1976 (D1) and 1999–2013 (D3)), and two warm (positive) phases (1977–1998 (D2) and 2014–2019 (D4)). The last warm phase might not have completed yet. These positive and negative phases are also the same as the PDO, indicating that the PDV index represents very well the Pacific basin-wide decadal variability.

To detect the recent change in the spatial pattern of the PDV, we compare the differences in the anomalous annual mean SST between the two PDV cycles (Figures 1b and 1c). During the first PDV cycle (1961–1998, Cycle 1 hereafter), the warm-minus-cold phase (D2-D1) features an equatorially symmetric SSTA pattern: a pair of abnormal cyclonic circulations residing over the North and South Pacific and an east-west contrasting SST anomaly with warming in the eastern Pacific and cooling in the western Pacific (Figure 1b). However, during the recent epoch (1999–2019, Cycle 2), the warm-minus-cold phase (D4-D3) features an equatorially asymmetric pattern between the North and South Pacific (Figure 1c). The cooling over the Kuroshio-Oyashio extension (KOE) and

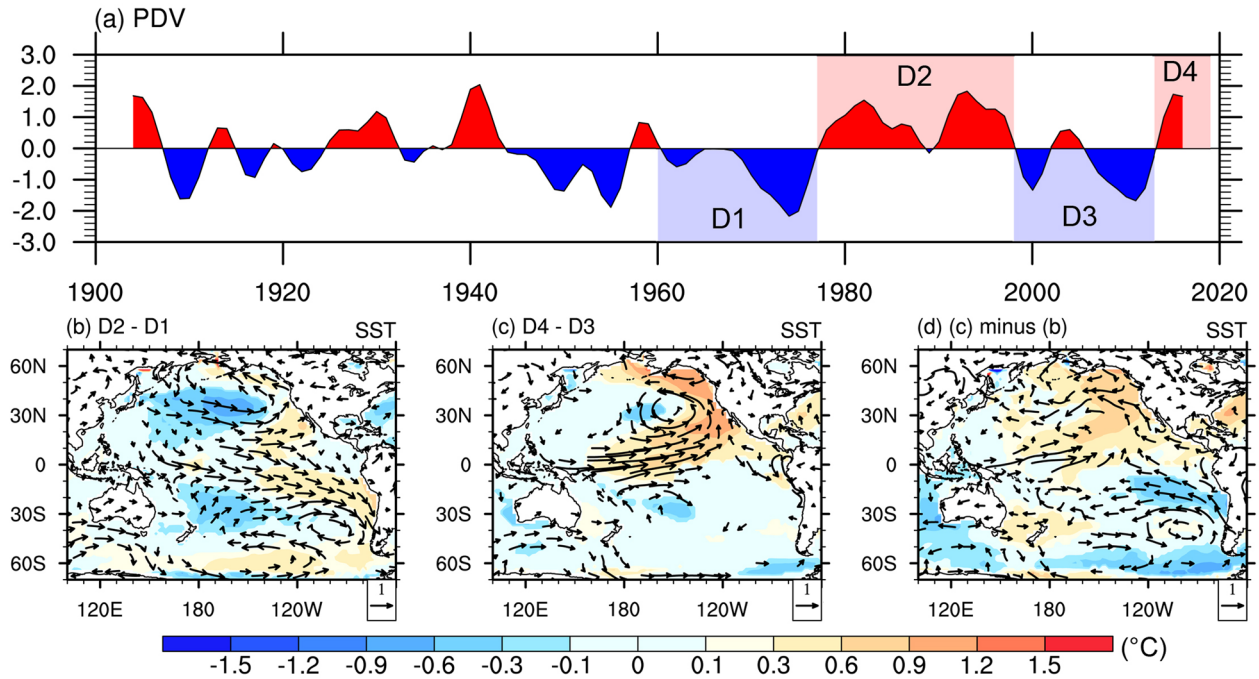

Figure 1. The observed change in the Pacific Decadal Variability (PDV) mode. (a) The time series of 7-year low-passed annual mean PDV index. Blue shadings represent the period 1961–1976 (D1) and 1999–2013 (D3), while red shadings represent the period 1977–1998 (D2) and 2014–2019 (D4). (b and c) represent the differences in detrended annual mean sea surface temperature anomalies (SSTA) (shadings, °C) and 850 hPa wind anomalies (vectors, m s^{-1}) for D2 minus D1 and D4 minus D3, respectively. (d) Denotes the results in (c) minus (b). Only the anomalies with a confidence level exceeding 90% (via a two-tailed Student's *t*-test) are displayed in (b and c). Only the absolute values of SST and wind anomalies larger than one standard deviation during 1961–2019 are shown in (d).

South Pacific convergence zone significantly weakens. Meanwhile, the horseshoe-like warming in the eastern North Pacific strengthens and the warming over the equatorial eastern Pacific has disappeared (Figure 1c). The corresponding anomalous cyclone shifts southeastward over the North Pacific and disappears over the eastern South Pacific. The PDV in the South Pacific considerably weakens in Cycle 2 (Figure 1d). The difference pattern between the Cycle 1 and Cycle 2 shows an overall "North Pacific warming—South Pacific cooling" pattern (Figure 1d).

The composite warm-minus-cold phase of the PDV during 1961–1998 (Figure 1b) bears a close similarity to the leading EOF mode of Pacific SSTA during the same period (Figure 2e). Likewise, the D4-D3 of the PDV during 1999–2019 (Figure 1c) resembles the leading EOF mode of Pacific SSTA during the same period (Figure 2g). It suggests that the leading EOF mode has changed around 1999 from the equatorially symmetric pattern to the asymmetric pattern. We note that the leading EOF mode has little change from 1901 to 1960 to 1961–1997 (Figures 2c and 2e), suggesting that the recent change of the PDV after 1999 is unique over the past 120 years. Notably, the amplitude of South Pacific SSTA decreases drastically during the D3 and D4 compared with those during the D1 and D2 (Figures 3a–3d).

Figure 3 suggests the impacts of the PDV's warm and cold phases and the changes of the impacts from Cycle 1 to Cycle 2. Overall, the warm and cold phases of PDV show opposite precipitation anomalies for both cycles. However, there are notable changes in the amplitude and spatial distribution of precipitation anomalies under the influence of PDV from Cycle 1 to Cycle 2. These changes are quantified by the area-averaged "warm-minus-cold phase" precipitation, that is, D2-D1 and D4-D3, over six regions of pronounced anomalies (Figures 3e–3j). First, precipitation anomalies have dramatically increased from Cycle 1 to Cycle 2, about tripled in all regions examined. Second, the precipitation anomaly's signs have reversed over tropical Africa, East Asia, and northern Siberia-Alaska from Cycle 1 to Cycle 2 (Figures 3e, 3g and S1 in Supporting Information S1), suggesting a spatial pattern change in the PDV's influence. Overall, the second cycle has a stronger impact and altered pattern on global land precipitation compared to those in the first cycle.

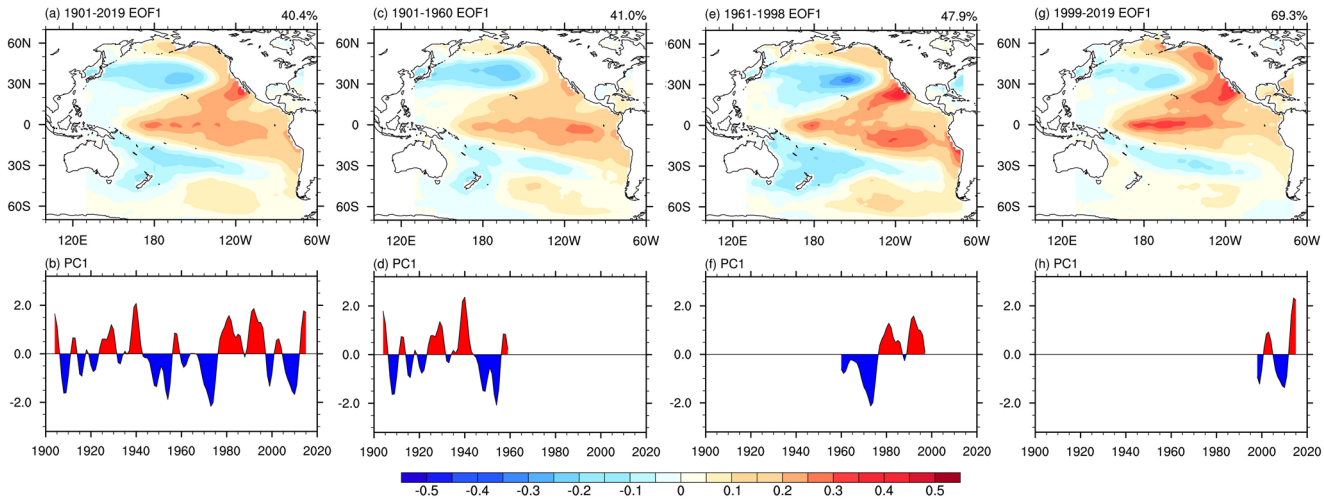

Figure 2. The 7-year low-passed annual mean Pacific Decadal Variability pattern. (a) The empirical orthogonal function (EOF1) of Pacific sea surface temperature during 1901-2019. (b) The PC1 of EOF analysis during 1901–2019. (c, d, e, f, g and h) same as (a and b), but for during 1901–1960, 1961–1998, and 1999–2019, respectively.

It should be noted that the two peaks during D2 seem to roughly correspond to the two strong El Niño events in 1982–1983 and 1997–1998 and the strong 2015–2016 El Niño also occurs during D4 (Figure 1a), which might contribute to the substantial SSTA in the Southeastern Pacific and corresponding anomalous circulation (e.g., Guan et al., 2014; Terray, 2011). We further checked the warm phase of PDV excluding the years of three strong El Niño events, that is, 1982–1983, 1997–1998, and 2015–2016 (Figure S2 in Supporting Information S1), and found that the results of SST, precipitation, and 850 hPa winds can be similar to Figures 3b and 3d.

The result indicates that the teleconnection derived from the twentieth century's PDV, used for the current decadal prediction of the land precipitation, can no longer apply in the current cycle. In addition to the impact on the precipitation, the enhanced northeastern Pacific PDV has drastically increased the amplitude and frequency of the marine heatwaves during the recent warm PDV phase since 2014 (Amaya et al., 2020; Di Lorenzo & Mantua, 2016).

4. Potential Influence of the External Forcings and Internal Variability

What might influence the PDV's change with the reduced variability in the northwestern and South Pacific and the increased variability in the North Pacific horseshoe region? We hypothesized that the PDV change might be affected by a combination of GHGs forcing and internal climate variability.

4.1. GHGs Forcing

We first examine historical simulation results to investigate the possible impact of external forcings on the recent SST decadal variability by contrasting the decadal standard deviation (STD) between 1999–2014 and 1961–1998. The observed SST decadal STD decreases over the western North Pacific and the southwest and southeast Pacific while increases along the west coast of North America (Figure 4a). Figure 4 also presents the corresponding simulation results derived from 33 CMIP6 models' multi-model ensemble mean (MMEM) of the historical runs (Figure 4b) and two individual sensitivity runs from 13 CMIP6 models' MMEM under single GHGs and NAT forcing (Figures 4c and 4d). These MMEM results largely eliminated internal variability, representing the forced responses of the PDV. The historical experiments capture the decreased decadal SST variability over the central North Pacific and South Pacific and the NH-SH asymmetry (Figure 4b) but cannot simulate the increased STD over the northeast Pacific.

The sensitive experiment results suggest that the GHGs forcing weakens the SST decadal variability, especially in the South Pacific and the tropical western North Pacific, resulting in the NH-SH asymmetry (Figure 4c). The differences in the MMEM EOF1 between 1999–2014 and 1961–1998 also suggests a weakened PDV pattern,

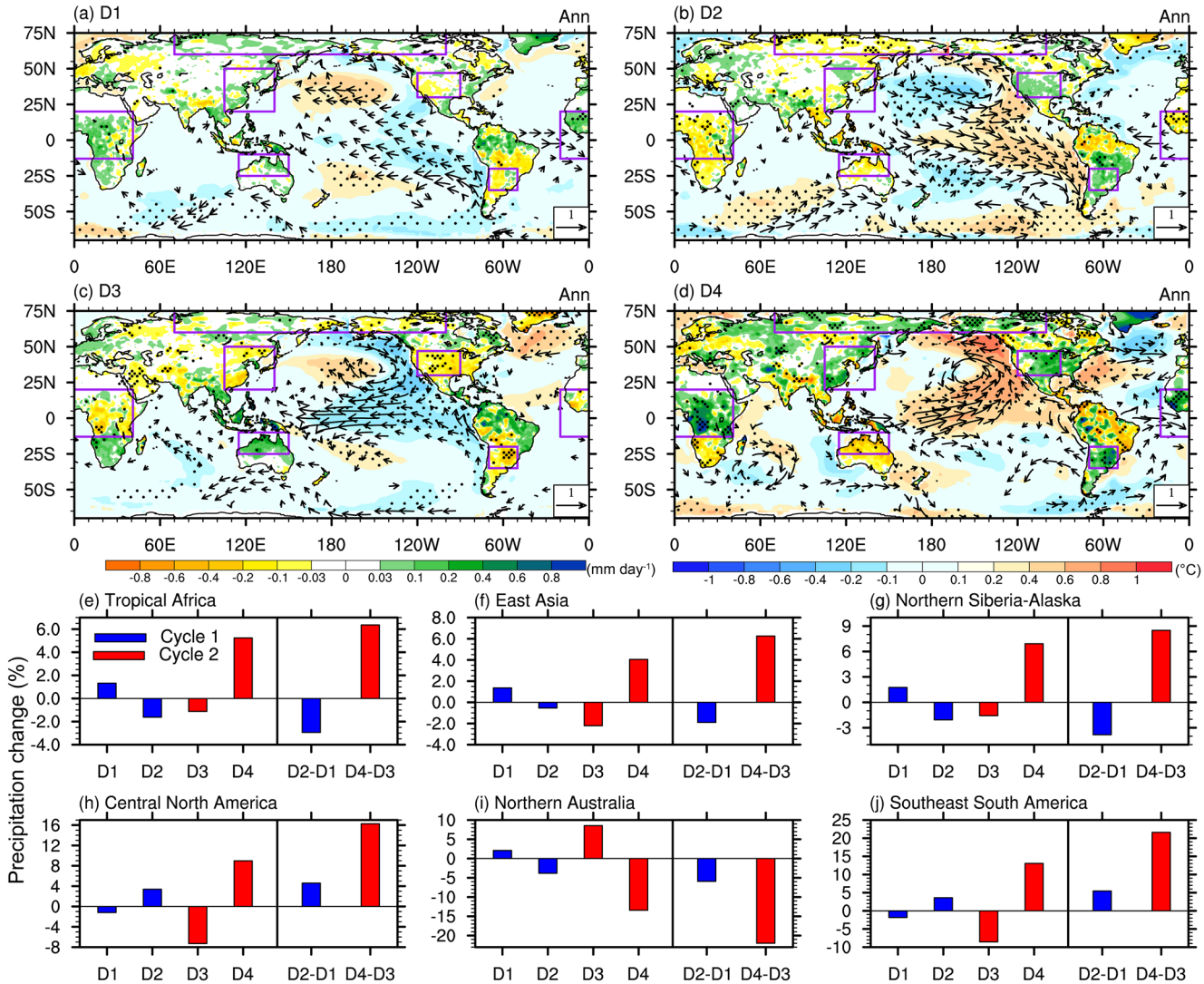

Figure 3. Change in the PDV's impact on precipitation and atmospheric circulation. (a–d) The anomalous annual mean 850 hPa winds (vectors, m s^{-1}), land precipitation (shading over the land, mm/day), and sea surface temperature (shading over the ocean, °C) for (a) D1, (b) D2, (c) D3, and (d) D4, relative to 1961–2019. The winds are masked over the land. The dots denote the significance at 90% confidence level (two-tailed Student's *t*-test), while only the vectors with a confidence level exceeding 90% are displayed. Precipitation change rate (%) in (e) tropical Africa, (f) East Asia, (g) northern Siberia-Alaska, (h) central North America, (i) northern Australia, and (j) southeast South America during the D1, D2, D3, and D4, relative to 1961–2019, and for D2 minus D1 and D4 minus D3, respectively. The purple boxes in (a–d) indicate the domains of these regions.

featuring positive anomalies over the KOE region and negative anomalies over the eastern South Pacific and southern Pacific Ocean along 60°S (Figures 5d–5f). We also checked the difference of PDV pattern in the GHGs run during 1999-2014 and in the PI-control run (Figure S3 in Supporting Information S1), and found a similar weakened PDV, which further confirms the effect of GHGs. Some previous studies suggested that natural external forcing (i.e., volcanic eruption and solar activity) may affect the SST variability in the Pacific (e.g., Liu et al., 2018; Sun et al., 2019, 2022). We found that the recent natural forcing mainly reduces the SST decadal variability over the North Pacific (Figure 4d), and the EOF1 difference pattern shows an enhanced PDV over the South Pacific, especially over the tropical central-eastern South Pacific and southern Pacific Ocean along 60°S (Figures 5a–5c). The above results together suggest that the observed recent PDV change bears a fingerprint of GHGs in the extratropical North and South Pacific, with a stronger influence in the South Pacific. However, the PDV change in the subtropical and extratropical eastern North Pacific is little affected by external forcing.

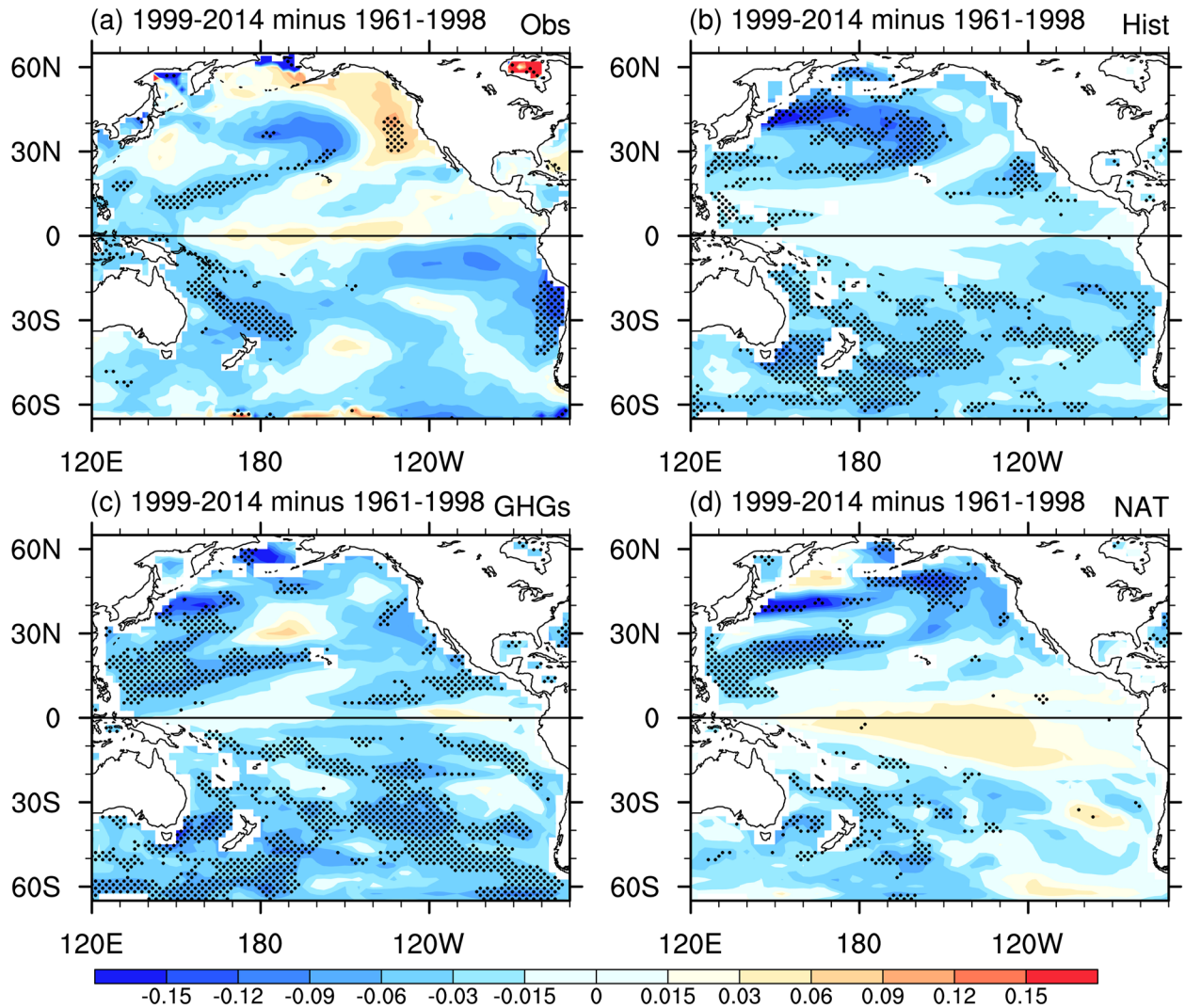

Figure 4. Differences in the standard deviation (STD) of 7-year low-passed detrended sea surface temperature (1999–2014 minus 1961–1998 means). (a–d) Results from the observations, Coupled Model Intercomparison Project Phase 6 historical, greenhouse gases (GHGs), and natural (NAT) scenarios, respectively. Note that only 13 models can be downloaded in the GHGs and NAT scenarios. The dots denote the STD differences that are significant at the 90% confidence level (*F* test) in (a), while they denote the agreement by at least 66% of the individual models in (b–d).

To better identify the response of the decadal SST variability to GHGs forcing, we further compare 33 models' future projections under the SSP5-8.5 scenario with the historical runs. The result shows that the PDV amplitude decreased under the GHGs-induced warming nearly everywhere in the Pacific Ocean (Figures 5g–5i). Notably, the PDV weakens more significantly over the South Pacific than the North Pacific. Corroborating with the reduced variance, the power spectrum peaks of the PDV at about 14–17 years in the historical scenarios are reduced by 20.5% and shifts to a marginal peak of 12–13 years in the SSP5-8.5 runs (Figure S4 in Supporting Information S1). Examination of the PDV in the North Pacific (0°–70°N) and South Pacific (0°–70°S) basins separately shows that the South Pacific PDV's amplitude decreased more than the North Pacific, and the South Pacific PDV's period shifts from 14 to 16 years toward a higher frequency in the SSP5-8.5. The shortening period occurred in 23 out of 33 models (70%). These results suggest that the GHGs forcing weakens the PDV variance and amplitude and shortens the PDV periodicity. It does not change the PDV spatial structure but creates the NH-SH asymmetry.

Previous studies found a weakened decadal SST variability over the North Pacific under greenhouse warming, which was related to the accelerated westward propagation of oceanic Rossby waves (Zhang & Delworth, 2016). In this study, we used the CMIP6 simulations and also found the stronger upper-ocean stratification and increased

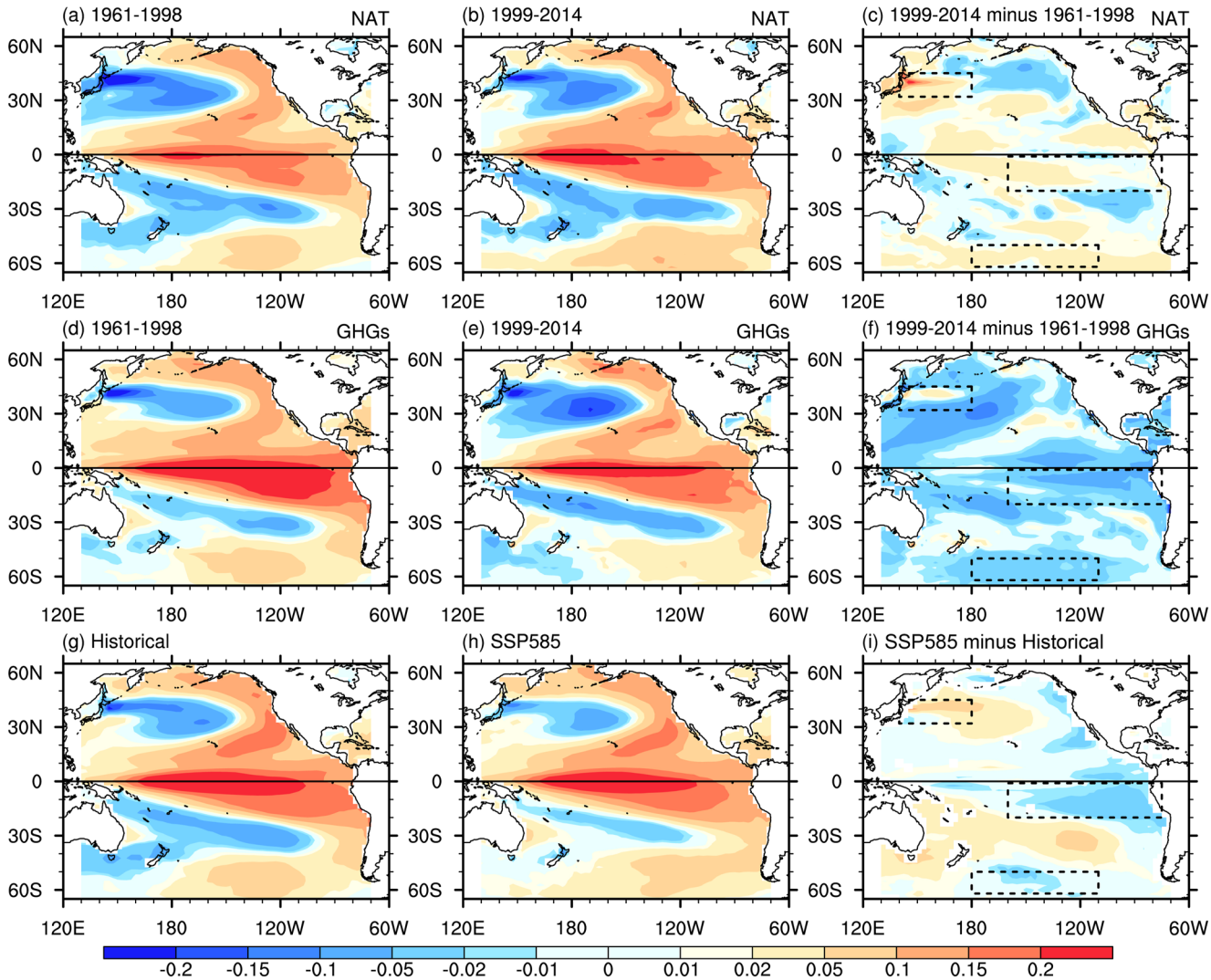

Figure 5. Simulated change in the spatial pattern of Pacific Decadal Variability (PDV) (a–c) under natural (NAT), (d–f) greenhouse gases (GHGs) (g–i) forcings and future greenhouse warming. The multimodel ensemble mean of the EOF1 from NAT scenarios during 1961-1998 (a) and 1999–2014 (b). (c) The EOF1 difference between (b) and (a). (d)-f) Are the same as (a)-c), but for the results from GHGs scenarios. The multimodel ensemble mean of the empirical orthogonal function (EOF1) from (g) 33 Coupled Model Intercomparison Project Phase 6 models under the historical and (h) SSP5-8.5 conditions. (i) The EOF1 difference between the SSP5-8.5 and the Historical runs. The corresponding PC1 in each model is normalized, and each EOF1 pattern is multiplied by the PC1's standard deviation, and thus the EOF1 pattern can indicate the Pacific Decadal Variability's amplitude. The dashed boxes denote the regions of Kuroshio-Oyashio Extension, eastern South Pacific and southern Pacific Ocean along 60°S.

buoyancy frequency over the North Pacific, causing the faster speed of westward-propagating Rossby waves (Figures 6b and 6d). Additionally, an increased buoyancy frequency also occurs over the South Pacific (Figure 6a). The accelerated Rossby waves are found at all latitudes over the South Pacific, and the MMEM acceleration is approximately 20% in the mid-latitude region (Figure 6c), which is similar to that over the North Pacific. The speed-up of off-equatorial westward-propagating Rossby waves may modulate the ocean gyre circulation and reduce the cross-basin time scale in the entire Pacific (Qiu & Chen, 2006; Wang et al., 2007), which might play an important role in shortening the lifespan and reducing the magnitude of the PDV.

Thus, the MMEM results suggest that the GHGs forcing weakens the PDV over the entire Pacific, (Figures 4c and 5i), which has a potential impact on the observed weakened PDV amplitude over the KOE region and South Pacific since 1999 (Figure 1c). However, the observed enhanced PDV over the eastern North Pacific and equatorial central Pacific cannot be simulated by external forcing experiments (Figure 4b), which means that internal variability might be responsible for it.

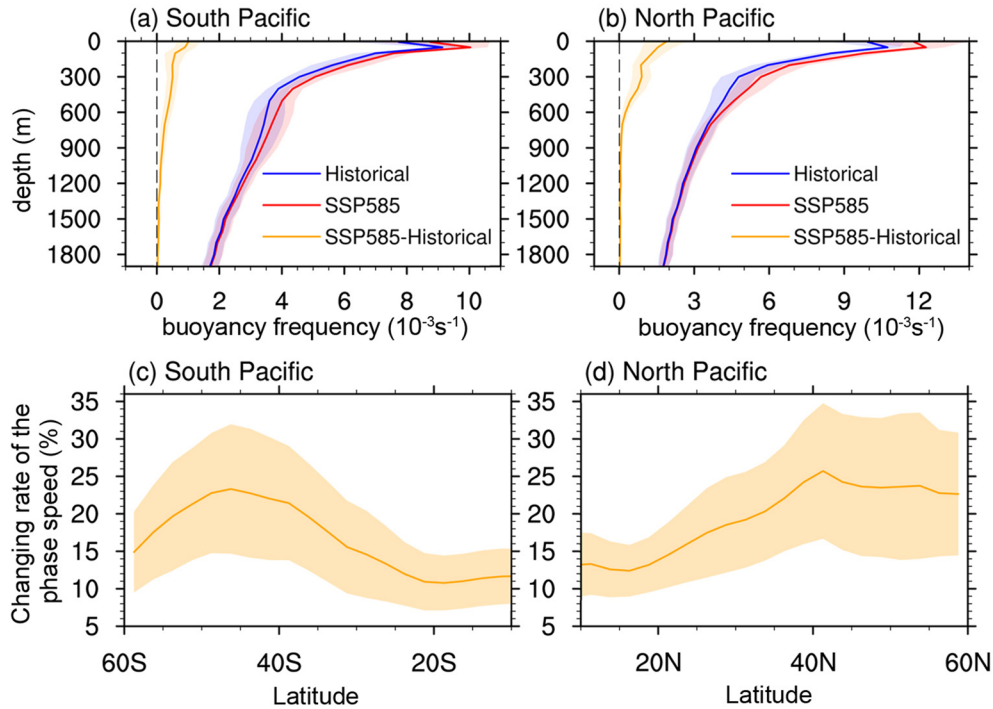

Figure 6. Simulated change in buoyancy frequency and Rossby wave speed. (a) The buoyancy frequency (10^{-3} s^{-1}) over the South Pacific region (10°S–60°S, 140°E−70°W) under the Historical (blue), SSP5-8.5 (red), and SSP5-8.5 minus historical (orange) conditions. (b) Same as (a), but for over the North Pacific region (10°N–60°N, 120°E−100°W). (c) The change rate of the zonally averaged first-baroclinic Rossby wave speed (m s^{-1}) over the South Pacific region between the SSP5-8.5 and the Historical condition. The phase speed is negative over the Pacific, which denotes westward propagation. (d) Same as (c), but for over the North Pacific region. Shading represents twice the standard deviation.

4.2. Internal Variability

We use the pre-industrial experiments from CMIP6 models, in which the external forcings are fixed, to examine the effects of internal variability. To show the magnitude of SST over the North Pacific in a more straightforward way, we characterize the horseshoe-shape pattern of the North Pacific PDV (NPDV) using two components. They are the averaged SSTA over the western NPDV (W-NPDV; 30°N–40°N, 180°–150°W) and eastern NPDV (E-NPDV; 10°N–20°N, 160°W–120°W) regions, respectively. The difference between E-NPDV and W-NPDV indices is highly correlated with the NPDV during 1901–2019, with a correlation coefficient of 0.93 ($p < 0.01$). Here the NPDV index is the leading EOF of the NP decadal variations derived from observation. Therefore, the difference between these two components can represent the NPDV change. Then the positive and negative phases of the NPDV can be represented by the positive and negative values of the E-NPDV minus W-NPDV indices, respectively.

To investigate if the internal variability could induce the strengthened PDV over the North Pacific horseshoe region, we select the events with the absolute value of the E-NPDV index is greater than that of the W-NPDV index. We then conduct the composite analysis between the NPDV positive and negative phases (Figure 7a). The result shows significant warming along the west coast of North America, subtropical eastern North Pacific, and the equatorial central Pacific, whereas a weak cooling over the KOE region. The simulated PDV resembles the observed North Pacific SST pattern during 1999–2019 (Figure 1c). Over the South Pacific, the SST pattern simulated by pre-industrial experiments is similar to the observed SST pattern during 1961–1998 (Figure 1b). Meanwhile, all models indicate that the occurrence of this SST pattern is possible, and the MMEM probability of that pattern is about 34.7% (Figure 7b).

Previous studies found that the tropical SST change (i.e., ENSO) could be a remote forcing for the decadal SST variability over the North Pacific (e.g., Alexander, 1992; Vimont et al., 2001; Deser et al., 2012; Newman et al., 2016). Since there is a significant equatorial central Pacific warming during the strengthened E-NPDV

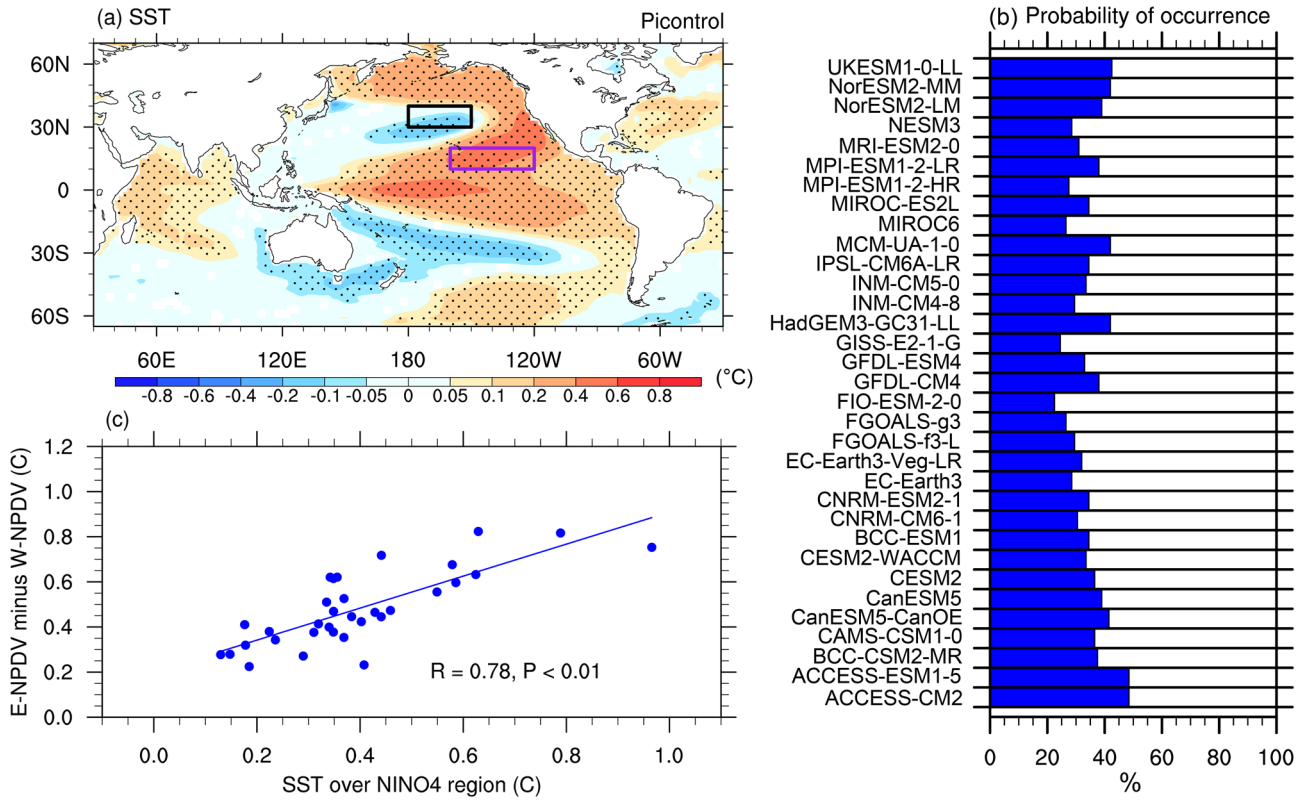

Figure 7. The effect of internal variability on North Pacific eastern boundary and equatorial central Pacific. (a) Composite analysis of decadal sea surface temperature (SST) change between the North Pacific Decadal Variability (NPDV) positive and negative phases in the multi-model ensemble mean pre-industrial-control experiments, and the absolute value of the E-NPDV index is greater than that of the W-NPDV index in each phase. The positive and negative phases of the NPDV are computed by E-NPDV minus W-NPDV indices greater than 0 and less than 0, respectively. The dots denote agreement by at least 66% of the individual models. The purple box represents the E-NPDV region (10°N–20°N, 160°W–120°W), while the black box denotes the W-NPDV region (30°N–40°N, 180°–150°W). All data are 7-year low-passed filtered before analysis. (b) Probability of occurrence of this SST pattern during the 200 years in each model. (c) Inter-model relationship between the anomalous SST over the Niño 4 region (5°N–5°S, 160°E−150°W) and E-NPDV minus W-NPDV indices during the occurrence of this SST pattern. The blue dots indicate the individual models.

mode (Figure 7a), we further examine the inter-model relationship between the anomalous SST over the Niño 4 region (5°N–5°S, 160°E−150°W) and the E-NPDV minus W-NPDV indices. The increased SST is found over the Niño 4 region in all 33 models, and the inter-model correlation is statistically significant ($r = 0.78$, $P < 0.01$) (Figure 7c), suggesting that the occurrence of central Pacific-ENSO (CP-ENSO) acts an important forcing for the enhanced decadal variability over the North Pacific eastern boundary. Observations show that there is more frequent occurrence of CP-ENSO after 1999 (e.g., Chung & Li, 2013; Wang et al., 2019), which may contribute to the recent enhanced variability over the North Pacific eastern boundary (Figure 1c). However, climate model simulations suggest that the future warming may also enhance the CP-ENSO variability (e.g., Kim & Yu, 2012), which means that the GHGs forcing may influence the internal variability. In this study, the MMEM results suggest that the overall influence of GHGs forcing will cause the weakened PDV, including the North Pacific eastern boundary (Figures 4c and 5i). Distinguishing the contribution of CP-ENSO variability change under future warming on the E-NPDV mode can be a future work.

Therefore, these findings suggest that internal variability (CP-ENSO) might produce the observed enhanced PDV over the North Pacific eastern boundary since 1999.

5. Concluding Remarks

This study reveals that the recent PDV cycle has distinctive characteristics and climate impacts from the PDV cycles in the twentieth century. We also use the CMIP6 modeling results to determine the attribution of external forcings and internal variability on the PDV change. The main findings are summarized as follows:

1. The PDV has experienced a notable change at the turn of the 21st century. This PDV change occurs mainly over the North Pacific with enhanced decadal variability over the North Pacific horseshoe region and reduced decadal variability in the KOE region and South Pacific
2. The recent PDV's cycle has significantly increased the amplitude of the global land precipitation anomalies over tropical Africa, northern Australia, East Asia, central North America, southern South America, and sub-Arctic regions. It also reversed the rainfall anomalies over tropical Africa, East Asia, and sub-Arctic regions
3. The CMIP6 simulations suggest that the GHGs forcing may have contributed to the recent PDV change by weakening the PDV amplitude over the KOE region, the South Pacific around 60°S, and the subtropical eastern South Pacific. The CMIP6 future projections also suggest that the GHGs forcing can weaken the PDV's amplitude and the PDV periodicity by increasing speed of oceanic Rossby waves, and create an NH-SH asymmetric pattern by suppressing the PDV in the SH. However, it does not explain the observed PDV's enhancement over the North Pacific horseshoe region
4. The control experiments suggest that internal variability might enhance the PDV over the North Pacific eastern boundary while decrease over the KOE region, which is related to the occurrence of CP-ENSO. Thus, the recent PDV change may be influenced by the combination of greenhouse warming and internal climate variability

There can be some uncertainties in the impacts of the PDV's warm and cold phases from Cycle 1 to Cycle 2 (Figure 3) because in spite of a same phase of PDV, the spatial structure of SST anomalies outside Pacific is not the same, which may also influence the precipitation and atmospheric circulation in the globe. The specific impact of this part needs to be considered in future research. Climate models might also have some uncertainties in the decadal predictions, especially for the limited skill in the over the central and northeastern Pacific region, where the models might miss or misrepresent mechanisms (Power et al., 2021). Moreover, some previous observational evidence and model experiments indicated that the KOE variability will increase in a warmer climate (e.g., Joh & Di Lorenzo, 2019; Qiu et al., 2014) due to changes in subtropical wind stress forcing over the central Pacific. In this paper, we mainly investigated the decadal variability of the entire Pacific based on the PDV, rather than focusing on a regional scale with different periodic changes, which could be the reason for some inconsistencies and uncertainties.

Our findings promote a deeper understanding of the causes of the PDV change. It reveals that the PDV change could have remarkable impacts on global atmospheric circulation and precipitation. The results also shed light on the PDV's future change, offering helpful guidance for infrastructure planning, disaster mitigation, food security, and water resource management in the coming decades.

Conflict of Interest

The authors declare no conflicts of interest relevant to this study.

Data Availability Statement

Data used in this paper can be downloaded from the following: ERA-40 and ERA-5: https://www.ecmwf.int/en/forecasts/datasets/reanalysis-datasets/era5, HadISST: https://www.metoffice.gov.uk/hadobs/hadisst, ERSST: https://www.ncdc.noaa.gov/data-access/marineocean-data/extended-reconstructed-sea-surface-temperature-ersst-v5, GPCC: https://psl.noaa.gov/data/gridded/data.gpcc.html, CMIP6 data: https://esgf-node.llnl.gov/search/cmip6.

Acknowledgments
We thank the ECMWF, GPCC, ERSST, HadISST, and CMIP5/6 for providing the data set. This research is jointly supported by the National Natural Science Foundation of China (42130604, 42105044, 41971108, 42111530182, and 91437218), Program of Innovative Research Team of Jiangsu Higher Education Institutions of China, and Priority Academic Program Development of Jiangsu Higher Education Institutions (164320H116).

References

Alexander, M. A. (1992) Midlatitude atmosphere–ocean interaction during El Nino. Part I: The North Pacific Ocean. *Journal of Climate*, *5*, 944–958. https://doi.org/10.1175/1520-0442(1992)005<0944:MAIDEN>2.0.CO;2

Alexander, M. A., Blade, I., Newman, M., Lanzante, J. R., Lau, N.-C., & Scott, J. D. (2002) The atmospheric bridge: The influence of ENSO teleconnections on air–sea interaction over the global oceans. *Journal of Climate*, *15*, 2205–2231. https://doi.org/10.1175/1520-0442(2002)015<2205:TABTIO>2.0.CO;2

Amaya, D. J., Miller, A. J., Xie, S.-P., & Kosaka, Y. (2020). Physical drivers of the summer 2019 North Pacific marine heatwave. *Nature Communications*, *11*, 1903. https://doi.org/10.1038/s41467-020-15820-w

Chelton, D. B., deSzoeke, R. A., Schlax, M. G., Naggar, K. E., & Siwertz, N. (1998). Geographical variability of the first baroclinic Rossby radius of deformation. *Journal of Physical Oceanography*, *28*, 433–460. https://doi.org/10.1175/1520-0485(1998)028<0433:gvotfb>2.0.co;2

Cheng, L., Trenberth, K. E., Fasullo, J., Boyer, T., Abraham, J., & Zhu, J. (2017). Improved estimates of ocean heat content from 1960 to 2015. *Science Advances*, *3*, e1601545. https://doi.org/10.1126/sciadv.1601545

Choi, J., An, S.-I., Yeh, S.-W., & Yu, J.-Y. (2013). ENSO-like and ENSO-induced tropical Pacific decadal variability in CGCMs. *Journal of Climate*, *26*, 1485–1501. https://doi.org/10.1175/JCLI-D-12-00118.1

Chung, P., & Li, T. (2013). Interdecadal relationship between the mean state and El Niño types. *Journal of Climate*, *26*, 361–379. https://doi.org/10.1175/JCLI-D-12-00106.1

Dai, A. (2013). The influence of the inter-decadal Pacific oscillation on US precipitation during 1923-2010. *Climate Dynamics*, *41*, 633–646. https://doi.org/10.1007/s00382-012-1446-5

Deser, C., Phillips, A., & Hurrell, J. W. (2004). Pacific interdecadal climate variability: Linkages between the Tropics and North Pacific during boreal winter since 1900. *Journal of Climate*, *17*, 3109–3124. https://doi.org/10.1175/1520-0442(2004)017<3109:picvlb>2.0.co;2

Deser, C., Phillips, A. S., & Tomas, R. (2012). ENSO and Pacific decadal variability in the community climate system model version 4. *Journal of Climate*, *25*, 2622–2651. https://doi.org/10.1175/JCLI-D-11-00301.1

Di Lorenzo, E., Cobb, K. M., Furtado, J. C., Schneider, N., Anderson, B. T., Bracco, A., et al. (2010). Central Pacific El Niño and decadal climate change in the North Pacific Ocean. *Nature Geoscience*, *3*, 762–765. https://doi.org/10.1038/ngeo984

Di Lorenzo, E., & Mantua, N. (2016). Multi-year persistence of the 2014/15 North Pacific marine heatwave. *Nature Climate Change*, *6*, 1042–1047. https://doi.org/10.1038/nclimate3082

Eyring, V., Bony, S., Meehl, G. A., Senior, C. A., Stevens, B., Ronald, S., et al. (2016). Overview of the Coupled Model Intercomparison Project Phase 6 (CMIP6) experimental design and organization. *Geoscientific Model Development*, *9*, 1937–1958. https://doi.org/10.5194/gmd-9-1937-2016

Geng, T., Yang, Y., & Wu, L. (2019). On the mechanisms of Pacific decadal oscillation modulation in a warming climate. *Journal of Climate*, *32*, 1443–1459. https://doi.org/10.1175/JCLI-D-18-0337.1

Guan, Y., Huang, B., Zhu, J., Hu, Z., & Kinter, J. (2014). Interannual variability of the South Pacific Ocean in observations and simulated by the NCEP climate forecast system, version 2. *Climate Dynamics*, *43*, 1141–1157. https://doi.org/10.1007/s00382-014-2148-y

Hartmann, D. L. (2015). Pacific Sea surface temperature and the winter of 2014. *Geophysical Research Letters*, *42*, 1894–1902. https://doi.org/10.1002/2015GL063083

Hersbach, H., de Rosnay, P., Bell, B., Schepers, D., Simmons, A., Soci, C., et al. (2018). *Operational global reanalysis: Progress, future directions and synergies with NWP ECMWF ERA Rep Series 2018; N27*. Retrieved from https://www.ecmwf.int/node/18765

Hu, Z.-Z., Kumar, A., Jha, B., Zhu, J., & Huang, B. (2017). Persistence and predictions of the remarkable warm anomaly in the northeastern Pacific Ocean during 2014-2016. *Journal of Climate*, *30*, 689–702. https://doi.org/10.1175/JCLI-D-16-0348.1

Huang, B., Thorne, P. W., Banzon, V. F., Boyer, T., Chepurin, G. A., Lawrimore, J. H., et al. (2017). Extended Reconstructed Sea surface temperature, version 5 (ERSSTv5): Upgrades, validations, and intercomparisons. *Journal of Climate*, *30*, 8179–8205. https://doi.org/10.1175/JCLI-D-16-0836.1

Hus, H.-H., & Chen, Y.-L. (2011). Decadal to bi-decadal rainfall variation in the western Pacific: A footprint of South Pacific Decadal variability? *Geophysical Research Letters*, *38*, L03703. https://doi.org/10.1029/2010GL046278

Joh, Y., & Di Lorenzo, E. (2019). Extension and central tropical pacific lead to preferred decadal-timescale oscillations in Pacific climate. *Scientific Reports*, *9*, 13558. https://doi.org/10.1038/s41598-019-49927-y

Kim, S. T., & Yu, J.-Y. (2012). The two types of ENSO in CMIP5 models. *Geophysical Research Letters*, *39*, L11704. https://doi.org/10.1029/2012GL052006

Kwon, M., Yeh, S.-W., Park, Y.-G., & Lee, Y.-K. (2013). Changes in the linear relationship of ENSO-PDO under the global warming. *International journal of climatology*, *33*, 1121–1128. https://doi.org/10.1002/joc.3497

Kwon, Y. O., & Deser, C. (2007). North Pacific Decadal variability in the community climate system model version 2. *Journal of Climate*, *20*, 2416–2433. https://doi.org/10.1175/JCLI4103.1

Li, S., Wu, L., Yang, Y., Geng, T., Cai, W., Gan, B., et al. (2020). The Pacific Decadal Oscillation less predictable under greenhouse warming. *Nature Climate Change*, *10*, 30–34. https://doi.org/10.1038/s41558-019-0663-x

Liguori, G., & Di Lorenzo, E. (2018). Meridional modes and increasing Pacific decadal variability under anthropogenic forcing. *Geophysical Research Letters*, *45*, 983–991. https://doi.org/10.1002/2017GL076548

Liu, F., Xing, C., Sun, L., Wang, B., Chen, D., & Liu, J. (2018). How do tropical, Northern Hemispheric, and Southern Hemispheric volcanic eruptions affect ENSO under different initial ocean conditions? *Geophysical Research Letters*, *45*, 13041–13049. https://doi.org/10.1029/2018GL080315

Liu, W., Xie, S.-P., & Lu, J. (2016). Tracking ocean heat uptake during the surface warming hiatus. *Nature Communications*, *7*. https://doi.org/10.1038/ncomms10926

Liu, Z. (2012). Dynamics of interdecadal climate variability: A historical perspective. *Journal of Climate*, *25*, 1963–1995. https://doi.org/10.1175/2011JCLI3980.1

Liu, Z., & Di Lorenzo, E. (2018). Mechanisms and predictability of Pacific decadal variability. *Current Climate Change Reports*, *4*, 128–144. https://doi.org/10.1007/s40641-018-0090-5

Lyman, J. M., Good, S. A., Gouretski, V., Ishii, M., Johnson, G. C., Palmer, M. D., et al. (2012). Robust warming of the global upper ocean. *Nature*, *465*, 334–337. https://doi.org/10.1038/nature09043

Lyon, B., Barnston, A. G., & DeWitt, D. G. (2014). Tropical Pacific forcing of a 1998–1999 climate shift: Observational analysis and climate model results for the boreal spring season. *Climate Dynamics*, *43*, 893–909. https://doi.org/10.1007/s00382-013-1891-9

Mantua, N. J., Hare, S., Zhang, Y., Wallace, J. M., & Francis, R. C. (1997). A Pacific interdecadal climate oscillation with impacts on salmon production. *Bulletin of the American Meteorological Society*, *78*, 1069–1079. https://doi.org/10.1175/1520-0477(1997)078<1069:apicow>2.0.co;2

Mo, K. C. (2000). Relationships between low-frequency variability in the southern hemisphere and sea surface temperature anomalies. *Journal of Climate*, *13*, 3599–3610. https://doi.org/10.1175/1520-0442(2000)013<3599:rblfvi>2.0.co;2

Newman, M., Alexander, M. A., Ault, T. R., Cobb, K. M., Deser, C., Di Lorenzo, E., et al. (2016). The Pacific Decadal Oscillation, revisited. *Journal of Climate*, *29*, 4399–4427. https://doi.org/10.1175/JCLI-D-15-0508.1

Power, S., Gasey, T., Folland, C. K., Colman, A., & Mehta, V. M. (1999). Inter-decadal modulation of the impact of ENSO on Australia. *Climate Dynamics*, *15*, 319–324. https://doi.org/10.1007/s003820050284

Power, S., Lengaigne, M., Capotondi, A., Khodri, M., Vialard, J., Jebri, B., et al. (2021). Decadal climate variability in the tropical Pacific: Characteristics, causes, predictability, and prospects. *Science*, *374*, eaay9165. https://doi.org/10.1126/science.aay9165

Qin, M., Li, D., Dai, A., Hua, W., & Ma, H. (2018). The influence of the Pacific Decadal Oscillation on North Central China precipitation during boreal autumn. *International Journal of Climatology*, *38*, 821–831. https://doi.org/10.1002/joc.5410

Qiu, B., & Chen, S. (2006). Decadal variability in the large-scale Sea Surface height field of the South Pacific Ocean: Observations and causes. *Journal of Physical Oceanography*, *36*, 1751–1762. https://doi.org/10.1175/JPO2943.1

Qiu, B., Chen, S., & Schneider, N. (2014). A coupled decadal prediction of the dynamic state of the Kuroshio extension system. *Journal of Climate*, *27*, 1751–1764. https://doi.org/10.1175/JCLI-D-13-00318.1

Rayner, N. A., Parker, D., Horton, E. B., Folland, C. K., Alexander, L., Rowell, D. P., et al. (2003). Global analyses of sea surface temperature, sea ice, and night marine air temperature since the late nineteenth century. *Journal of Geophysical Research*, *108*, 447. https://doi.org/10.1029/2002JD002670

Schneider, N., Miller, A. J., & Pierce, D. W. (2002). Anatomy of North Pacific decadal variability. *Journal of Climate*, *15*, 586–605. https://doi.org/10.1175/1520-0442(2002)015<0586:aonpdv>2.0.co;2

Schneider, U., Becker, A., Finger, P., Meyer-Christoffer, A., Ziese, M., & Rodolf, B. (2014). GPCC's new land surface precipitation climatology based on quality-controlled in situ data and its role in quantifying the global water cycle. *Theoretical and Applied Climatology*, *115*, 15–40. https://doi.org/10.1007/s00704-013-0860-x

Seager, R., Hoerling, M., Schubert, S., Wang, H., Lyon, B., Kumar, A., et al. (2015). Causes of the 2011-2014 California drought. *Journal of Climate*, *28*, 6997–7024. https://doi.org/10.1175/JCLI-D-14-00860.1

Sun, W., Liu, J., Wang, B., Chen, D., & Gao, C. (2022). Pacific Multidecadal (50–70 year) variability instigated by volcanic forcing during the Little Ice Age (1250–1850). *Climate Dynamics*. https://doi.org/10.1007/s00382-021-06127-7

Sun, W., Liu, J., Wang, B., Chen, D., Liu, F., Wang, Z., et al. (2019). A "La Niña-like" state occurring in the second year after large tropical volcanic eruptions during the past 1500 years. *Climate Dynamics*, *52*, 7495–7509. https://doi.org/10.1007/s00382-018-4163-x

Terray, P. (2011). Southern hemisphere extra-tropical forcing: A new paradigm for El Niño-southern Oscillation. *Climate Dynamics*, *36*, 2171–2199. https://doi.org/10.1007/s00382-010-0825-z

Uppala, S. M., Kallberg, P., Simmons, A. J., Andrae, U., Bechtold, V., Fiorino, M., et al. (2005). The ERA-40 re-analysis. *Quarterly Journal of the Royal Meteorological Society*, *131*, 2961–3012. https://doi.org/10.1256/qj.04.176

Van Oldenborgh, G. J., Doblas-Reyes, F. J., Wouters, B., & Hazeleger, W. (2012). Decadal prediction skill in a multi-model ensemble. *Climate Dynamics*, *38*, 1263–1280. https://doi.org/10.1007/s00382-012-1313-4

Vimont, D. J., Battisti, S., & Hirst, A. C. (2001). Footprinting: A seasonal connection between the tropics and mid-latitudes. *Geophysical Research Letters*, *28*, 3923–3926. https://doi.org/10.1029/2001GL013435

Wang, B., Luo, X., Yang, Y., Sun, W., Cane, M. A., Cai, W., et al. (2019). Historical change of El Niño properties sheds light on future changes of extreme El Niño. *Proceedings of the National Academy of Sciences of the United States of America*, *116*, 22512–22517. https://doi.org/10.1073/pnas.1911130116

Wang, S.-Y. S., Huang, W., & Yoon, J. H. (2015). the North American winter "dipole" and extremes activity: A CMIP5 assessment. *Atmospheric Science Letters*, *16*, 338–345. https://doi.org/10.1002/asl2.565

Wang, X., Li, C., & Zhou, W. (2007). Interdecadal mode and its propagating characteristics of SSTA in the South Pacific. *Meteorology and Atmospheric Physics*, *98*, 115–124. https://doi.org/10.1007/s00703-006-0235-2

Whitney, F. A. (2014). Anomalous winter winds decrease 2014 transition zone productivity in the NE Pacific. *Geophysical Research Letters*, *42*, 428–431. https://doi.org/10.1002/2014GL062634

Wu, L., Cai, W., Zhang, L., Nakamura, H., Timmermann, A., Joyce, T., et al. (2012). Enhanced warming over the global subtropical western boundary currents. *Nature Climate Change*, *2*, 161–166. https://doi.org/10.1038/nclimate1353

Zhang, L. P., & Delworth, T. L. (2016). Simulated response of the Pacific Decadal Oscillation to climatic change. *Journal of Climate*, *29*, 5999–6018. https://doi.org/10.1175/JCLI-D-15-0690.1

Zhang, Y., Xie, S.-P., Kosaka, Y., & Yang, J.-C. (2018). Pacific Decadal Oscillation: Tropical Pacific forcing versus internal variability. *Journal of Climate*, *31*, 8265–8279. https://doi.org/10.1175/JCLI-D-18-0164.1

Zhong, Y., Liu, Z., & Jacob, R. (2008). Origin of Pacific multidecadal variability in community climate system model, version 3 (CCSM3): A combined statistical and dynamical assessment. *Journal of Climate*, *21*, 114–133. https://doi.org/10.1175/2007JCLI1730.1